An Ion Mobility-Mass Spectrometry Imaging Workflow

Daniela Mesa Sanchez[1], Steve Creger[1†],Veerupaksh Singla[2†], Ruwan T. Kurulugama[3], John Fjeldsted[3], Julia Laskin[1]

[1]Department of Chemistry, Purdue University, West Lafayette, IN 47906, USA

[2]Department of Chemical Engineering, Indian Institute of Technology Bombay, Powai, Mumbai, Maharashtra 400076, India

[3]Agilent Technologies Inc., Santa Clara, CA 95051, USA

Abstract: Mass spectrometry imaging (MSI) is a powerful technique for the label-free spatially-resolved analysis of biological tissues. Coupling ion mobility (IM) separation with MSI allows separation of isobars in the mobility dimension and increases confidence of peak assignments. Recently, imaging experiments have been implemented on the Agilent 6560 Ion Mobility Quadrupole Time of Flight Mass Spectrometer, making MSI experiments more broadly accessible to the MS community. However, the absence of data analysis software for this system presents a bottleneck. Herein, we present a vendor-specific imaging workflow to visualize IM-MSI data produced on the Agilent IM-MS system. Specifically, we have developed a Python script, the ion mobility-mass spectrometry image creation script (IM-MSIC), which interfaces Agilent's Mass Hunter Mass Profiler software with the MacCoss lab's Skyline software and generates drift time and mass-to-charge selected ion images. In the workflow, Mass Profiler is used for an untargeted feature detection. The IM-MSIC script mediates user input of data and extracts ion chronograms utilizing Skyline's command-line interface, then proceeds towards ion

† Undergraduate student researchers.

image generation within a single user interface. Ion image post-processing is subsequently performed using different tools implemented in accompanying scripts.

Introduction:

Mass spectrometry imaging (MSI) is a powerful technique that enables simultaneous label-free analysis of hundreds of spatially localized molecules in complex samples[1–8]. Commonly, these samples are biological tissues and thus the analyte mixture is composed of lipids and metabolites present in a wide range of concentrations. Ion mobility (IM) is a separation approach that separates the analytes on the basis of size, shape and charge and hence provides the ability of isomer and isobar differentiation[9]. The improved signal-to-noise ratio and peak capacity that results from ion mobility separations are especially beneficial to the analysis of isomers and low abundance metabolite peaks otherwise occluded by interferences[10,11]. An extensive body of work already couples front-end separations with ion mobility and mass spectrometry[12]. Subsequently, workflows have been developed to account for the ion mobility dimension of these datasets[13].

More recently, several ion mobility-mass spectrometry imaging experiments have been reported. These include whole body and brain tissue imaging utilizing matrix-assisted laser desorption ionization (MALDI)[14–16]. Ambient techniques including laser-assisted electrospray ionization (LAESI)[17], desorption electrospray ionization (DESI)[6], and most recently, infrared matrix-assisted laser desorption electrospray ionization (IR-MALDESI)[18] also have been employed. Although commercial IM-MSI systems with accompanying software exist, support for custom implementations of MSI on IM instruments is limited. For these types of implementations individual m/z and drift time ion peaks are isolated manually using custom scripts[17], or through targeted lists using a modified version of MSiReader[18]. Herein, we present a semi-automated untargeted data analysis workflow for imaging experiments using Agilent IM-Q-

TOF instrument and the generation of ion images with the mobility and mass-to-charge dimensions. This workflow extends the capabilities of Agilent's IM-Q-TOF instrument and facilitates the development of custom imaging platforms in support of untargeted analysis which to this point has not been well addressed in previous implementations.

Experimental:

The imaging data presented in this manuscript was acquired using a desorption electrospray ionization source prototype (DESI 2D, Prosolia, Indianapolis, IN) coupled to a 6560 IM-Q-TOF mass spectrometer (Agilent Technologies, Santa Clara, CA). A syringe pump (Fusion 100, Chemyx Inc., Stafford, TX) with a 2.5 mL Hamilton syringe was used to deliver a 3 µL/min flow of methanol. The spray head was positioned ~1 mm from the tissue surface at a 70° angle to generate a < 0.1 mm spray spot on the substrate. The spray tip and collection tube were set ~4 mm apart. The nebulizer nitrogen gas was 140 psi. The source drying gas temperature was 350 °C at a flow rate of 12 L/min. The VCap voltage was set to 4000V. The maximum drift time of the ion mobility drift tube was set to 46 ms with a 38 ms ion funnel trap time. The drift tube entrance and exit voltages were set to -1547 V and -224 V, respectively. Rear funnel entrance and exit were 217.5 V and -45 V, respectively. OmniSpray software (Prosolia) was used to control the DESI source, and a worklist in MassHunter data acquisition software was used to automate acquisition. Each line scan was saved as a single Agilent raw data file (.d). The image pixel resolution was set to 100 µm with a scan rate of 100 µm/s and 1 Hz data acquisition rate. Total acquisition time for one line was 4.2 min. The biological samples were 5-10 µm thick sagittal brain sections of spontaneous hypertensive stroke prone rats (Charles Rivers Labs, Wilmington, MA). Additionally,

plain slides with red marker circles were imaged for their characteristic rhodamine B peak (443.2391 *m/z*).

Results:

The data analysis workflow described in detail in the following sections is summarized in Figure 1 and can be downloaded at https://github.com/LabLaskin/IM-MSI-workflow. Briefly, the user generates an untargeted mass list from all or part of the imaging data set using Agilent's chemometric software, MassProfiler. A custom-designed script written in Python 3, the ion mobility-mass spectrometry image creator (IM-MSIC), is used to direct this mass list, along with the raw data files into Skyline[19]. Skyline is a freely available client application for reaction monitoring method development and targeted analysis of mass spectrometry data. Skyline allows for the quantitative analysis of the features identified by MassProfiler. The output provided by Skyline is subsequently processed using the IM-MSIC script, which constructs a matrix containing the abundances of drift time and mass-to-charge separated features and generates ion images. Ion images can be normalized either to the total ion current (TIC) or a user-defined ion image. Multiple data sets can be processed simultaneously. This workflow utilizes MassHunter Mass Profiler (Agilent Technologies, Santa Clara, CA) version B.08.01, Skyline-daily (MacCoss Labs, Seattle, WA) version 4.2.1.19058, and Skyline Runner. A number of freely-available Python packages are also used, including NumPy[20], Pandas[21], and Matplotlib[22].

Loading and Processing Data Files

Data processing in the Python workflow begins with analysis in MassProfiler. The user inputs all or some of the raw (.d) data files containing the individual imaging experiment lines into MassProfiler as a new project of a single group. Using Agilent's Molecular Feature Extraction

(MFE) algorithm and user defined parameters, a set of recurring molecular features identified by their *m/z* and IM drift time across all the data files are selected, aligned, and normalized. The stringency of selected parameters determines the number of detected features and necessary processing time. For data shown below we used the following constraints: 1) an infusion data input filter and an ion intensity cutoff of greater than or equal to 150 counts; 2) a common organic (no halogen) isotope model with a limit of charge states of 1-2; 3) disregard of single-ion features with a charge state of 1; 4) drift time tolerance of ±1.5% ; 5) mass tolerance of ±(15.0 ppm± 2.0 mDa); 6) max ion intensity as the measure of abundance. Furthermore, we included only those features that were present in 50% of sample lines. Using this approach, we extracted 559 features (S1) from 143 lines of the DESI-MSI data in 10 minutes using 8 Gb RAM on an Intel i7 (1.80 GHz, WIN10, 64-bit). Upon completion of molecular feature extraction, the feature summary containing all features is exported from the resulting MassProfiler result table and saved in the folder containing the raw data. At present, MassProfiler can be used to process multiple line scans simultaneously as a common group but does not support batch processing of multiple independent imaging data sets, only binary comparison. Thus, the MassProfiler analysis must be performed individually for each independent set of data preceding the batch-capable steps.

Next, we launch the IM-MSIC script, which opens a text-based interface that guides the user through generation of ion images for one or more experiments. Immediately, the user is prompted to modify the preferred settings, which also can be modified by editing the accompanying “SETTINGS” text file. The settings include the desired color map style, image format, and paths to Skyline Runner, the Skyline template file, and a default home directory for images created by the post-processing functions. Detailed description of the individual setting

112 options can be found in the usage notes in the supplementary information. The script opens a file
113 browser, which allows the user to pick a single or multiple data folders for processing. Each
114 directory should contain the raw data, in the form of individual line. d files, and its own
115 MassProfiler report as described previously. The user is then prompted to input the desired
116 aspect ratios of ion images for each experiment and whether they would like to generate drift
117 time and *m/z* selected ion images, or only *m/z* selected ion images. A numbered selection menu is
118 then presented for the user to indicate what type of normalization, if any, should be used. The
119 following options are currently included: 1) no normalization; 2) normalization to total-ion-
120 current (TIC); 3) normalization to the signal of internal standards or any other ion image. The
121 user is also provided with options to simultaneously generate ion images with multiple different
122 normalization schemes. If normalization to internal standards or other ion images is chosen, for
123 example, the user is queried for a comma separated list of identification values, which
124 correspond to the Mass Profiler report feature identification number of the features to be used.

125 Following this step, each experiment folder is independently processed by the IM-MSIC
126 script. It reformats the MassProfiler report into an appropriate Skyline transition list input format
127 generating a .csv file type and launches the Skyline command-line interface. A first-time-use
128 configuration of Skyline's transition and report settings is described in the user notes and is
129 modeled after previous usage of Skyline with Agilent IM-MS data[13]. The IM-MSIC script directs
130 unsupervised processes in Skyline for the import of raw data, extraction of individual
131 chronograms for every Mass Profiler-selected feature, export of the TIC and export of the final
132 report. The final report is then used to generate ion images for each feature and name the files
133 according to the corresponding *m/z* and drift time. Along with an image file (the format of which
134 can be adjusted in settings), a .txt file is produced which contains the raw intensities of each

pixel. For 559 unnormalized images made up of 143 individual data lines on 8 Gb RAM system with Intel i7 (1.80 GHz, WIN10, 64-bit) the entire processing time, excluding Mass Profiler feature extraction takes approximately 40 minutes. Given Skyline's multithreading capabilities, the time required for this operation can be significantly reduced by using more processing power.

Post-Processing

Absolute Comparison: Each ion image created by the main function is self-normalized (normalized to the highest signal of a particular feature) and therefore spans the entirety of the selected heat map color range. Thus, the heat map scale of each raw image is not directly comparable to that of any other ion image. Although self-normalization maximizes the intra-image contrast of compound localization in the tissue, especially in the case of low abundance ions, it impedes comparisons of multiple features or the same feature observed in multiple data sets on the basis of abundance. These abundance comparisons are particularly important when comparing the abundance of isomers separated by their mobility and comparing ion images of the same feature for different experiments. Thus, the "absolute comparison" tool regenerates a collection of ion images such that share a common color scale. This approach is illustrated in Figure 2, which shows two self-normalized ion images (Figure 2, "Raw.") and the same images displayed on a common color scale (Figure 2, "Processed"). This stand-alone script utilizes the .txt files generated by the main function. Upon launching the script, the user is given the option to change the main settings as in the main function (heat map style, image format, etc.). Next, the option of selecting individual files or folders is presented. If the individual files option is selected, the user chooses however many .txt files corresponding to the features of interest. If multiple experiment folders are selected, the script will rescale matching file names together,

158 generating ion images of the same feature across different experiments on a common color scale.
159 File names are considered matching within ±0.001 Da for mass-to-charge ratios and ±0.1 ms for
160 drift times by default, but these tolerances can be adjusted in the main settings.

161 RGB Overlay: In complex systems, multi-analyte colocalization or differential spatial
162 distribution might be of interest. In order to better visualize these relationships, it is common to
163 generate a composite image of multiple analyte ion images as shown in Figure 3. This is
164 achieved by assigning one of three analytes to each of the three color channels, red, green, and
165 blue (as seen at the top of Figure 3); overlapping regions appear as color combinations, while
166 non-overlapping regions depict the assigned color channel of an analyte. Upon launching the
167 dedicated script, the user is given the option to change the main settings as in the main function.
168 Next, a browser window allows the user to select three .txt files. The composite image is
169 generated, and the user is then prompted to create another image, save, or quit. It is important to
170 note, that each channel is self-normalized and therefore the intensities of different color channels
171 are not comparable.

172 Outlier Correction: Spike pixels are a possible occurrence in MSI data. These experimental
173 artifacts are detrimental to the overall image contrast given that one outlying intensity prevents
174 the utilization of the available color scale range. The spike correction script developed in this
175 study offers three main approaches to this issue illustrated in Figure 4, which shows the same ion
176 image unprocessed, and after three different types of spike correction processing. Figure 4a
177 shows unprocessed ion image obtained for *m/z*: 443.2123, t_D: 27.11 ms. This corresponds to the
178 rhodamine pigment of red marker. A single white pixel stands out while the rest of the image is
179 black and dark red. This underutilization of the full heat map range, points to a drastic difference
180 between intensities of this single white pixel and the rest of the image, i.e., a spike. The first

outlier correction approach (Figure 4B) simply attenuates the impact of a single high outlier by scaling down the intensity difference between the highest and second-highest intensities to a user-defined value. This enhances image contrast but does not alter the relative intensities of any other pixels in the ion image, which is always preferable. This sort of approach is most effective when only a single spike pixel exists in the image. The second approach (Figure 4C) determines outliers as pixels of intensity greater than $\mu + 3\sigma$, where μ is the mean intensity of all pixels in the image. Outliers intensities are replaced with the median of the 8 nearest neighbors. This approach can be effective when multiple spike pixels are present, but the determination of these outlying spike pixels may be biased by the inclusion of large portions of background surface and/or in cases where signal is tightly localized to a small region. In such cases, over processing can be a concern. Thus, this approach is generally best used for broad homogenous distributions. The third approach (Figure 4D) is derivative of the previous one, but rather than determining outliers based on the mean of all pixels in the image, it determines outliers based on the mean intensity of neighboring pixels. This helps combat the previously mentioned bias in spike determination. The number of neighboring pixels taken into consideration for outlier detection is a user-defined feature that can be tuned to a samples' feature sizes. Upon launching the outlier correction script, the user is prompted to select one or more of the .txt files generated alongside the images. The original image is recreated in the console and all three spike correction algorithms are offered as options. The corrected images are generated in-console and an option to save, try a different algorithm, or select a different file are presented.

Discussion:

The addition of ion mobility separation to MSI increases molecular coverage obtained in MSI experiments and presents an opportunity for higher rates of identification and/or higher

confidence in assignments. Currently, several databases exist which support this endeavor, including peptide[23,24], glycomics[25], lipid[26], and metabolite and small molecule[23,27,28] databases. A well-curated and standardized compilation of these can be found in the form of the Collision Cross Section (CCS) Compendium[29]. Moreover, various *in silico* predictors such as LipidCCS[26], MetCCS[30], DeepCCS[31], and CCSbase[32] are available. These databases rely on CCS values, which can be readily determined for ions observed in MSI experiments by acquiring a tune mix spectrum before, during and/or after an imaging experiment. Not only does CCS provide an additional parameter for the characterization and identification of molecules, it may also serve as the solution to drift time shift. Although the experimental data used in this study did not show significant drift time shifts overtime, it is possible for drift times to slightly vary over long acquisition periods. This is easily corrected by converting drift time values to CCS. Since MassProfiler and Skyline supports conversion to CCS, this workflow can be readily adapted to utilize CCS values instead of drift times for data processing.

One of the strengths of MSI lies in its label-free untargeted spatial localization of molecules in biological samples and one of its weaknesses is the lack of separation prior to analysis, which makes it difficult to identify the detected species. Ion mobility separation helps address the weakness of MSI by separating ions in the gas phase. Meanwhile, the untargeted data analysis workflow presented in this study may bolster the information gained from these experiments. Since feature selection is a standalone process, and Skyline provides multi-vendor support, it is also conceivable that this workflow can be adapted for an untargeted or targeted approach of data types other than the Agilent data format by using an alternate chemometric approach for feature selection.

Conclusion

Ion mobility is a powerful separation technique, which enhances the molecular coverage and provides an added dimension of molecular information in MSI experiments necessary for confident peak assignments. Herein, we have presented a workflow for the untargeted generation of drift time and m/z-selected ion images from IM-MSI data, particularly for an Agilent system. The workflow utilizes a Python script, which links MassProfiler and Skyline to generate ion images. This semi-automated approach parallels data import and extraction using multiple computing processes at a time to generate a large number of images in a relatively short amount of time. The IM-MSIC script as well as the supporting tools and user notes can be found at https://github.com/LabLaskin/IM-MSI-workflow.

Acknowledgements

This research is supported by the grant from the National Science Foundation (NSF-1808136). DMS acknowledges support from the National Science Foundation Graduate Research Fellowship under Grant No. (DGE-1333468). Any opinions, findings, and conclusions or recommendations expressed in this material are those of the authors and do not necessarily reflect the views of the National Science Foundation.

References

(1) Cornett, D. S.; Reyzer, M. L.; Chaurand, P.; Caprioli, R. M. MALDI Imaging Mass Spectrometry: Molecular Snapshots of Biochemical Systems. *Nat. Methods* **2007**, *4* (10), 828–833. https://doi.org/10.1038/nmeth1094.

(2) McDonnell, L. A.; Heeren, R. M. A. Imaging Mass Spectrometry. *Mass Spectrom. Rev.* **2007**, *26* (4), 606–643. https://doi.org/10.1002/mas.20124.

(3) Spengler, B. Mass Spectrometry Imaging of Biomolecular Information. *Anal. Chem.* **2015**, *87* (1), 64–82. https://doi.org/10.1021/ac504543v.

(4) Wu, C.; Dill, A. L.; Eberlin, L. S.; Cooks, R. G.; Ifa, D. R. Mass Spectrometry Imaging under Ambient Conditions. *Mass Spectrom. Rev.* **2013**, *32* (3), 218–243. https://doi.org/10.1002/mas.21360.

(5) Chughtai, K.; Heeren, R. M. A. Mass Spectrometric Imaging for Biomedical Tissue Analysis. *Chem. Rev.* **2010**, *110* (5), 3237–3277. https://doi.org/10.1021/cr100012c.

(6) Buchberger, A. R.; DeLaney, K.; Johnson, J.; Li, L. Mass Spectrometry Imaging: A Review of Emerging Advancements and Future Insights. *Anal. Chem.* **2018**, *90* (1), 240–265. https://doi.org/10.1021/acs.analchem.7b04733.

(7) Laskin, J.; Lanekoff, I. Ambient Mass Spectrometry Imaging Using Direct Liquid Extraction Techniques. *Anal. Chem.* **2016**, *88* (1), 52–73. https://doi.org/10.1021/acs.analchem.5b04188.

(8) Stoeckli, M.; Chaurand, P.; Hallahan, D. E.; Caprioli, R. M. Imaging Mass Spectrometry: A New Technology for the Analysis of Protein Expression in Mammalian Tissues. *Nat. Med.* **2001**, *7* (4), 493–496. https://doi.org/10.1038/86573.

(9) Kanu, A. B.; Dwivedi, P.; Tam, M.; Matz, L.; Hill, H. H. Ion Mobility–Mass Spectrometry. *J. Mass Spectrom.* **2008**, *43* (1), 1–22. https://doi.org/10.1002/jms.1383.

(10) Dwivedi, P.; Schultz, A. J.; Jr, H. H. H. Metabolic Profiling of Human Blood by High-Resolution Ion Mobility Mass Spectrometry (IM-MS). *Int. J. Mass Spectrom.* **2010**, *298* (1), 78–90. https://doi.org/10.1016/j.ijms.2010.02.007.

(11) Bennett, R. V.; Gamage, C. M.; Galhena, A. S.; Fernández, F. M. Contrast-Enhanced Differential Mobility-Desorption Electrospray Ionization-Mass Spectrometry Imaging of Biological Tissues. *Anal. Chem.* **2014**, *86* (8), 3756–3763. https://doi.org/10.1021/ac5007816.

(12) Zheng, X.; Wojcik, R.; Zhang, X.; Ibrahim, Y. M.; Burnum-Johnson, K. E.; Orton, D. J.; Monroe, M. E.; Moore, R. J.; Smith, R. D.; Baker, E. S. Coupling Front-End Separations, Ion Mobility Spectrometry, and Mass Spectrometry For Enhanced Multidimensional Biological and Environmental Analyses. *Annu. Rev. Anal. Chem.* **2017**, *10* (1), 71–92. https://doi.org/10.1146/annurev-anchem-061516-045212.

(13) MacLean, B. X.; Pratt, B. S.; Egertson, J. D.; MacCoss, M. J.; Smith, R. D.; Baker, E. S. Using Skyline to Analyze Data-Containing Liquid Chromatography, Ion Mobility Spectrometry, and Mass Spectrometry Dimensions. *J. Am. Soc. Mass Spectrom.* **2018**, *29* (11), 2182–2188. https://doi.org/10.1007/s13361-018-2028-5.

(14) Jackson, S. N.; Ugarov, M.; Egan, T.; Post, J. D.; Langlais, D.; Schultz, J. A.; Woods, A. S. MALDI-Ion Mobility-TOFMS Imaging of Lipids in Rat Brain Tissue. *J. Mass Spectrom.* **2007**, *42* (8), 1093–1098. https://doi.org/10.1002/jms.1245.

(15) McLean, J. A.; Ridenour, W. B.; Caprioli, R. M. Profiling and Imaging of Tissues by Imaging Ion Mobility-Mass Spectrometry. *J. Mass Spectrom.* **2007**, *42* (8), 1099–1105. https://doi.org/10.1002/jms.1254.

(16) Trim, P. J.; Henson, C. M.; Avery, J. L.; McEwen, A.; Snel, M. F.; Claude, E.; Marshall, P. S.; West, A.; Princivalle, A. P.; Clench, M. R. Matrix-Assisted Laser Desorption/Ionization-Ion Mobility Separation-Mass Spectrometry Imaging of Vinblastine in Whole Body Tissue Sections. *Anal. Chem.* **2008**, *80* (22), 8628–8634. https://doi.org/10.1021/ac8015467.

(17) Li, H.; Smith, B. K.; Márk, L.; Nemes, P.; Nazarian, J.; Vertes, A. Ambient Molecular Imaging by Laser Ablation Electrospray Ionization Mass Spectrometry with Ion Mobility Separation. *Int. J. Mass Spectrom.* **2015**, *377*, 681–689. https://doi.org/10.1016/j.ijms.2014.06.025.

(18) Ekelöf, M.; Dodds, J.; Khodjaniyazova, S.; Garrard, K. P.; Baker, E. S.; Muddiman, D. C. Coupling IR-MALDESI with Drift Tube Ion Mobility-Mass Spectrometry for High-Throughput Screening and Imaging Applications. *J. Am. Soc. Mass Spectrom.* **2020**, *31* (3), 642–650. https://doi.org/10.1021/jasms.9b00081.

(19) MacLean, B.; Tomazela, D. M.; Shulman, N.; Chambers, M.; Finney, G. L.; Frewen, B.; Kern, R.; Tabb, D. L.; Liebler, D. C.; MacCoss, M. J. Skyline: An Open Source Document Editor for Creating and Analyzing Targeted Proteomics Experiments. *Bioinformatics* **2010**, *26* (7), 966–968. https://doi.org/10.1093/bioinformatics/btq054.

(20) van der Walt, S.; Colbert, S. C.; Varoquaux, G. The NumPy Array: A Structure for Efficient Numerical Computation. *Comput. Sci. Eng.* **2011**, *13* (2), 22–30. https://doi.org/10.1109/MCSE.2011.37.
(21) McKinney, W. Data Structures for Statistical Computing in Python; 2010; pp 51–56.
(22) Hunter, J. D. Matplotlib: A 2D Graphics Environment. *Comput. Sci. Eng.* **2007**, *9* (3), 90–95. https://doi.org/10.1109/MCSE.2007.55.
(23) Lietz, C. B.; Yu, Q.; Li, L. Large-Scale Collision Cross-Section Profiling on a Traveling Wave Ion Mobility Mass Spectrometer. *J. Am. Soc. Mass Spectrom.* **2014**, *25* (12), 2009–2019. https://doi.org/10.1021/jasms.8b04673.
(24) Bush, M. F.; Hall, Z.; Giles, K.; Hoyes, J.; Robinson, C. V.; Ruotolo, B. T. Collision Cross Sections of Proteins and Their Complexes: A Calibration Framework and Database for Gas-Phase Structural Biology. *Anal. Chem.* **2010**, *82* (22), 9557–9565. https://doi.org/10.1021/ac1022953.
(25) Struwe, W. B.; Pagel, K.; Benesch, J. L. P.; Harvey, D. J.; Campbell, M. P. GlycoMob: An Ion Mobility-Mass Spectrometry Collision Cross Section Database for Glycomics. *Glycoconj. J.* **2016**, *33* (3), 399–404. https://doi.org/10.1007/s10719-015-9613-7.
(26) Zhou, Z.; Tu, J.; Xiong, X.; Shen, X.; Zhu, Z.-J. LipidCCS: Prediction of Collision Cross-Section Values for Lipids with High Precision To Support Ion Mobility–Mass Spectrometry-Based Lipidomics. *Anal. Chem.* **2017**, *89* (17), 9559–9566. https://doi.org/10.1021/acs.analchem.7b02625.
(27) Zheng, X.; Aly, N. A.; Zhou, Y.; Dupuis, K. T.; Bilbao, A.; Paurus, V. L.; Orton, D. J.; Wilson, R.; Payne, S. H.; Smith, R. D.; Baker, E. S. A Structural Examination and Collision Cross Section Database for over 500 Metabolites and Xenobiotics Using Drift Tube Ion Mobility Spectrometry. *Chem. Sci.* **2017**, *8* (11), 7724–7736. https://doi.org/10.1039/C7SC03464D.
(28) Hernández-Mesa, M.; Le Bizec, B.; Monteau, F.; García-Campaña, A. M.; Dervilly-Pinel, G. Collision Cross Section (CCS) Database: An Additional Measure to Characterize Steroids. *Anal. Chem.* **2018**, *90* (7), 4616–4625. https://doi.org/10.1021/acs.analchem.7b05117.
(29) Picache, J. A.; Rose, B. S.; Balinski, A.; Leaptrot, K. L.; Sherrod, S. D.; May, J. C.; McLean, J. A. Collision Cross Section Compendium to Annotate and Predict Multi-Omic Compound Identities. *Chem. Sci.* **2019**, *10* (4), 983–993. https://doi.org/10.1039/C8SC04396E.
(30) Zhou, Z.; Xiong, X.; Zhu, Z.-J. MetCCS Predictor: A Web Server for Predicting Collision Cross-Section Values of Metabolites in Ion Mobility-Mass Spectrometry Based Metabolomics. *Bioinformatics* **2017**, *33* (14), 2235–2237. https://doi.org/10.1093/bioinformatics/btx140.
(31) Plante, P.-L.; Francovic-Fontaine, É.; May, J. C.; McLean, J. A.; Baker, E. S.; Laviolette, F.; Marchand, M.; Corbeil, J. Predicting Ion Mobility Collision Cross-Sections Using a Deep Neural Network: DeepCCS. *Anal. Chem.* **2019**, *91* (8), 5191–5199. https://doi.org/10.1021/acs.analchem.8b05821.
(32) Ross, D. H.; Cho, J. H.; Xu, L. Breaking Down Structural Diversity for Comprehensive Prediction of Ion-Neutral Collision Cross Sections. *Anal. Chem.* **2020**, *92* (6), 4548–4557. https://doi.org/10.1021/acs.analchem.9b05772.

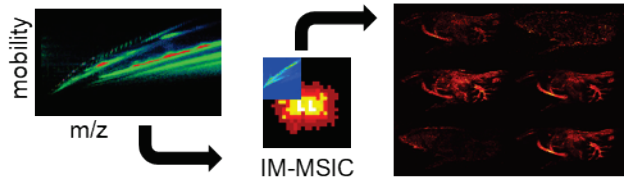

Graphical Abstract

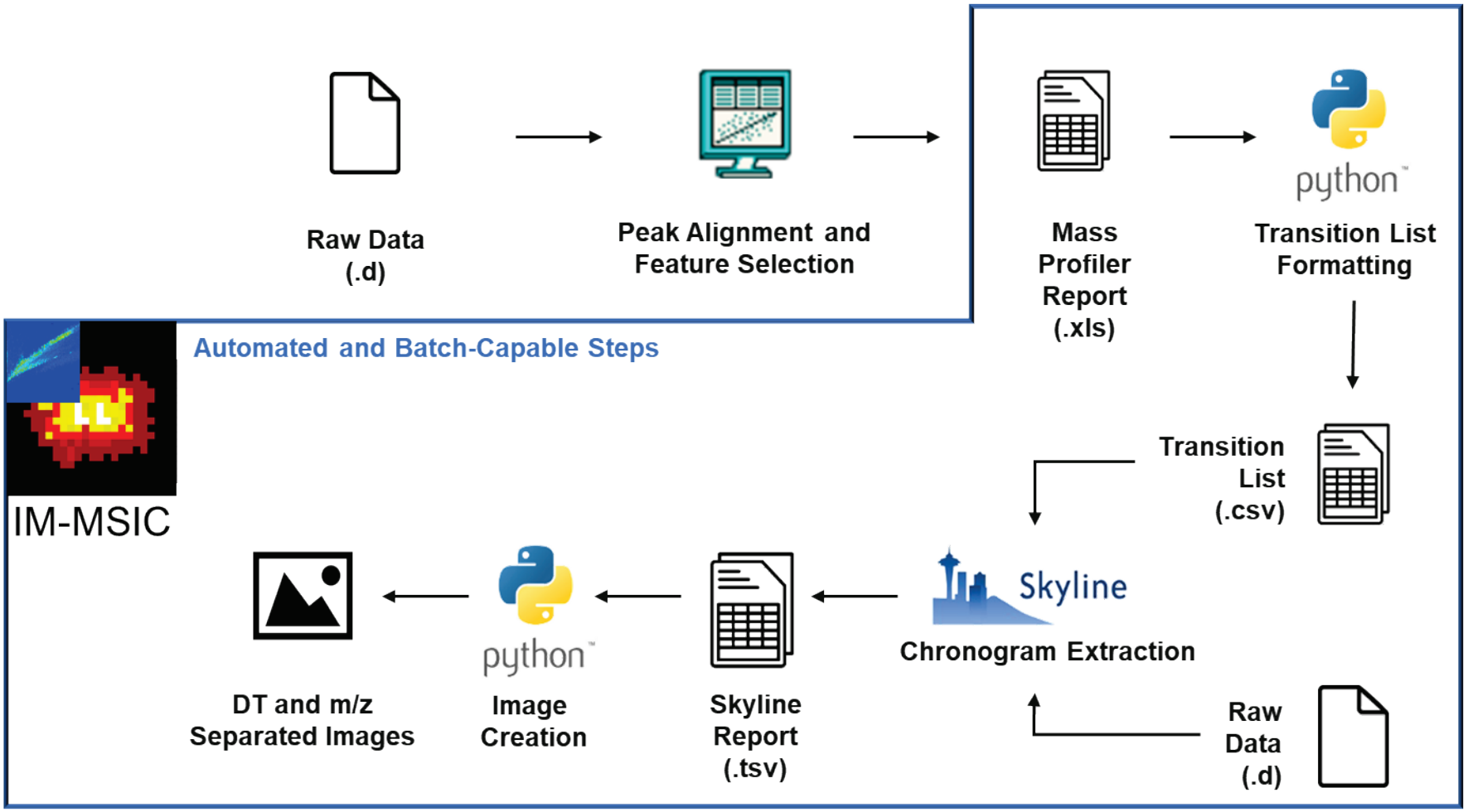

Figure 1: Graphical overview of file inputs and outputs of base processing steps. Steps outside the blue outline are user-supervised and do not presently support simultaneous processing of multiple datasets. Steps within the blue outline are directed by a Python script after initial user-selected settings and support analysis of multiple datasets at once.

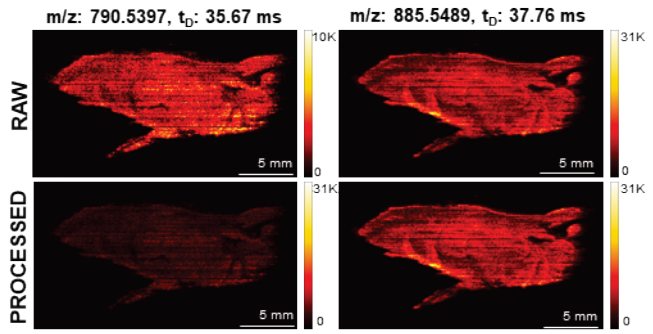

357

Figure 2: Absolute image comparison algorithm applied to peaks at *m/z*: 790.5397, t_D: 35.67 ms and *m/z*: 885.5489, t_D: 37.76 ms. While raw ion images utilize a self-normalized color scale to maximize image contrast; the algorithm generates images on a common color scale among two or more ion images.

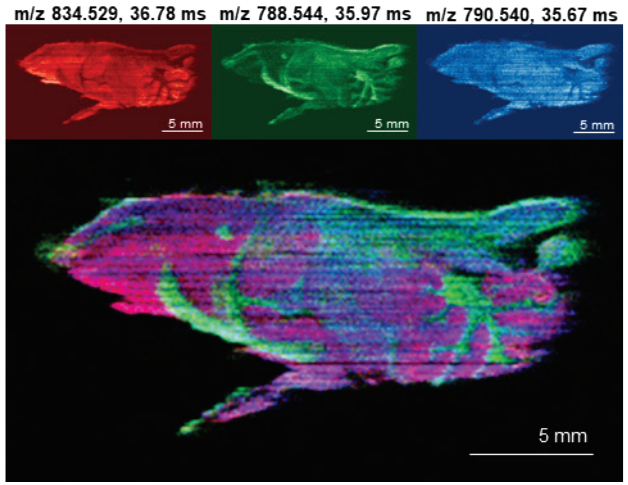

358

359

360

Figure 3: RGB Overlay function sample. Each pixel's Red, Green, and Blue value is determined by the intensity of a different compound to create a composite. In this case, a composite image of lipids PS(40:6), PS(36:1), and PE(40:6), as determined by exact mass, is presented.

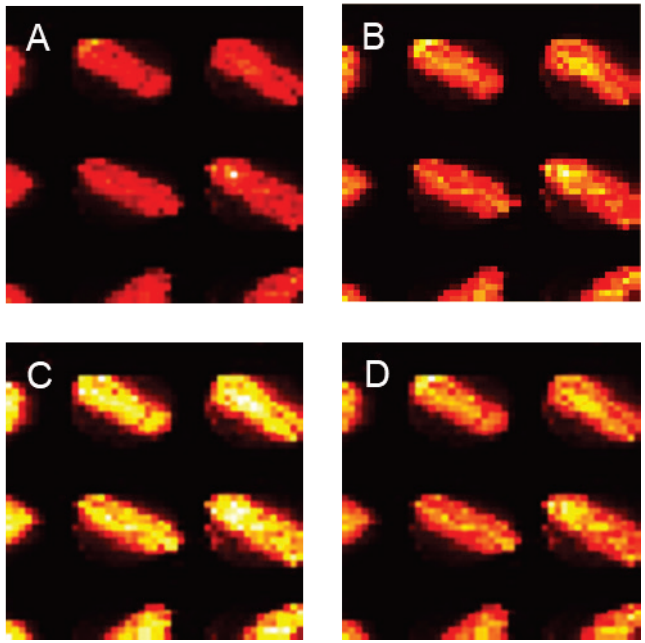

361

Figure 4: Spike correction algorithms applied on rhodamine spots (*m/z*: 443.2123, t_D: 27.11 ms). Panel A) shows default output. Panel B) depicts the attenuation algorithm, in which the highest peak is reduced making every other pixel appear brighter in comparison. Panel C) shows the output when outliers are selected based on the whole image average intensity and replaced with median of 8 closest neighbors. Similarly, the algorithm of panel D) selects outliers found by comparing against local mean intensity (as defined by the user), and replaces outliers with the median of 8 nearest neighbors.